

# Valley degeneracy breaking by magnetic field in monolayer MoSe<sub>2</sub>

David MacNeill, Colin Heikes, and Zachary Anderson  
*Department of Physics, Cornell University, Ithaca, NY 14853, USA*

Kin Fai Mak and Daniel C. Ralph  
*Department of Physics, Cornell University, Ithaca, NY 14853, USA and  
Kavli Institute at Cornell, Cornell University, Ithaca, NY 14853, USA*

Andor Kormányos  
*Department of Physics, University of Konstanz, D-78464 Konstanz, Germany*

Viktor Zólyomi  
*Department of Physics, Lancaster University, Lancaster LA1 4YB, United Kingdom*

Jiwoong Park  
*Department of Chemistry and Chemical Biology,  
Cornell University, Ithaca, NY 14853, USA and  
Kavli Institute at Cornell, Cornell University, Ithaca, NY 14853, USA*  
(Dated: July 2, 2022)

Using polarization-resolved photoluminescence spectroscopy, we investigate valley degeneracy breaking by out-of-plane magnetic field in back-gated monolayer MoSe<sub>2</sub> devices. We observe a linear splitting of  $-0.22 \frac{\text{meV}}{\text{T}}$  between luminescence peak energies in  $\sigma_+$  and  $\sigma_-$  emission for both neutral and charged excitons. The optical selection rules of monolayer MoSe<sub>2</sub> couple photon handedness to the exciton valley degree of freedom, so this splitting demonstrates valley degeneracy breaking. In addition, we find that the luminescence handedness can be controlled with magnetic field, to a degree that depends on the back-gate voltage. An applied magnetic field therefore provides effective strategies for control over the valley degree of freedom.

Monolayer MoSe<sub>2</sub> and other semiconducting monolayer transition metal dichalcogenides (TMDs) are a materials system with unique potential for controlling their valley degree of freedom [1–8]. Similar to graphene, the conduction and valence band show extrema (valleys) at the vertices of a hexagonal Brillouin zone; unlike graphene, MoSe<sub>2</sub> exhibits a nonzero optical gap of 1.66 eV [9, 10]. This has allowed exploration of optoelectronic properties arising from the valley-dependent chirality of massive Dirac fermions, predicted in the context of inversion symmetry broken graphene [11, 12]. This chirality leads to valley-contrasting orbital angular momenta, which result in optical selection rules coupling the exciton valley degree of freedom to photon handedness [2–7]. Using polarization-resolved spectroscopy researchers have demonstrated valley-selective luminescence with near 100% fidelity [2, 7]. Furthermore, the ability to pump valley-polarized carriers with circularly-polarized light has been demonstrated through the valley Hall effect [8]. Valley-dependent orbital angular momentum is also predicted to create a magnetic moment (termed the valley moment) coupling valley pseudospin to magnetic field [11–13], which opens up the possibility for magnetic control over the valley degree of freedom [13, 14].

Here, we demonstrate the use of magnetic fields to break valley degeneracy in a monolayer TMD. Specifically, we report polarization resolved luminescence spec-

tra for back-gated MoSe<sub>2</sub> devices at 4.2 K and in magnetic fields up to 6.7 T. We study the luminescence peak energies as a function of magnetic field, finding a linear splitting of  $-0.22 \frac{\text{meV}}{\text{T}}$  between peaks corresponding to light emission with different senses of circular polarization,  $\sigma_+$  and  $\sigma_-$ . We interpret this as a Zeeman splitting due to valley-dependent magnetic moments. We also investigate the field dependence of luminescence handedness, finding that the emission becomes polarized in field even with unpolarized excitation, and that the degree of this polarization can be increased to about 50% by gating the sample. This suggests the creation of valley population imbalance through the simultaneous application of magnetic and electric fields. Our results demonstrate a recently-proposed [14] strategy for generating valley populations, and could lead to new approaches for controlling the valley degree of freedom in monolayer TMDs.

Our device geometry and measurement apparatus are shown in Fig. 1a and 1b. All measurements were taken using a scanning confocal microscope integrated with a 7 T superconducting magnet dewar, with light coupled in and out of the system via a polarization-maintaining optical fiber (similar designs were reported in Refs. [15, 16]). The light is focused into a roughly 1  $\mu\text{m}$  diameter spot using a pair of aspheric lenses, and the sample is scanned using piezo-driven nanopositioners (from attocube). The sample, positioners, and optical components are placed in a vacuum cryostat which is then evacuated and lowered

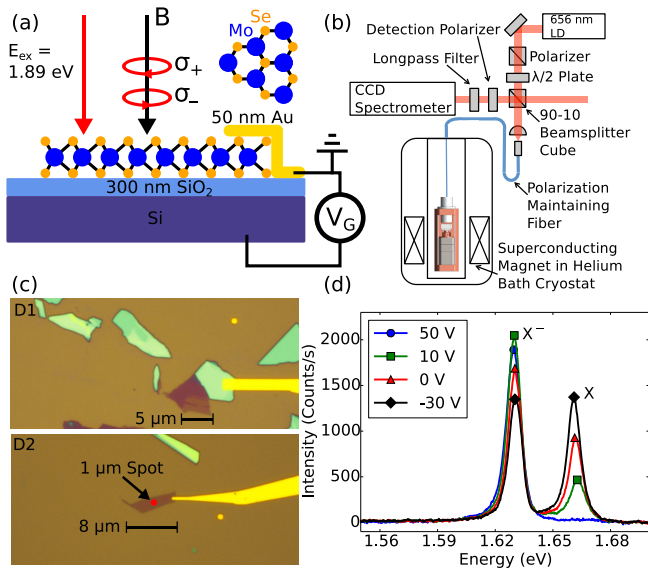


FIG. 1. (a) Experimental geometry showing back-gated monolayer MoSe<sub>2</sub> devices in out-of-plane magnetic fields. Luminescence is excited with light from a 1.89 eV laser diode and collected separately for  $\sigma_+$  and  $\sigma_-$  polarization in the Faraday geometry. The in-plane honeycomb lattice structure of MoSe<sub>2</sub> is shown in the upper right. (b) Schematic of the fiber-coupled optical cryostat used in the experiment. (c) Optical micrographs of devices D1 and D2. (d) Luminescence spectra of D2 taken at 0 T and 4.2 K with -30 V, 0 V, 10 V, and 50 V back gate voltage.

into a helium bath containing a superconducting magnet; helium exchange gas is added to ensure thermalization of the sample at 4.2 K. For the data in the main text, the excitation power was between 10-60  $\mu$ W to reduce possible heating effects.

To enable polarization-resolved spectroscopy, a zero-order quartz  $\lambda/4$  plate is placed between the aspheric lenses, oriented at 45° to the fiber axes; this couples  $\sigma_+$  and  $\sigma_-$  emission into orthogonal polarization modes of the fiber. The light exiting the fiber is directed through a rotatable polarizer, which selects one fiber mode for spectral analysis by a thermoelectrically cooled CCD spectrometer. We can also create circularly polarized excitation by coupling linearly polarized light into one of the two fiber polarization modes, or create equal intensity excitation in  $\sigma_+$  and  $\sigma_-$  polarization by coupling in light polarized at 45° to the fiber axes. We excite photoluminescence with light from a 1.89 eV laser diode, which is 230 meV blueshifted from the A exciton transition, and as a result we see very little dependence of the emission polarization on excitation polarization (see supplement section 1). The conclusions discussed below are independent of excitation polarization.

To fabricate our samples, we exfoliate bulk MoSe<sub>2</sub> crystals (grown by direct vapor transport) onto 300 nm sili-

con oxide on silicon, then use electron-beam lithography to define a single 0.5 nm Ti/50nm Au contact, allowing use of the silicon substrate as a back gate. All data shown in the main text were taken from devices D1 and D2 pictured in Fig. 1c. Figure 1d shows the  $B = 0$  luminescence spectra of D2 at -30 V, 0 V, 10 V, and 50 V. The peaks at 1.66 eV and 1.63 eV correspond to the neutral and charged A exciton respectively, with a charged exciton (trion) binding energy of 30 meV [9]. As the back gate voltage is increased the exciton luminescence decreases and the trion luminescence increases, showing that our samples are intrinsically  $n$ -type and the 1.63 eV peak corresponds to negatively charged trion luminescence.

Figure 2a compares polarization-resolved spectra taken for D1 in out-of-plane magnetic fields of 0 T, 6.7 T and -6.7 T and with the back gate grounded. For this data, we excite photoluminescence using equal intensity excitation in  $\sigma_+$  and  $\sigma_-$  polarization. At zero field, we find no significant dependence of the peak energies or intensities on emission handedness. In comparison, the spectra taken at 6.7 T show splitting between the  $\sigma_+$  and  $\sigma_-$  emission peaks of about -1.5 meV for both the exciton and trion. The luminescence is also  $\sigma_+$  polarized: the trion peak has  $P_{\text{trion}} = \frac{I_+ - I_-}{I_+ + I_-} = 14\%$ , where  $I_{\pm}$  is the peak intensity of the trion in  $\sigma_{\pm}$  detection. For the exciton we measure  $P_{\text{exciton}} = 9\%$ . The polarization changes sign with reversal of the magnetic field, showing that it arises from magnetically induced changes in the exciton and trion populations. Figure 2b depicts the schematic band structure of a MoSe<sub>2</sub> monolayer, illustrating the direct band gaps at the  $K_+$  and  $K_-$  points, with arrows indicating the allowed A exciton transitions for  $\sigma_{\pm}$  light. Since the emission handedness is coupled to the exciton valley degree of freedom, the peak splitting and polarization we observe indicate valley degeneracy breaking.

Figure 3a shows the valley splitting of the exciton and trion peaks, defined as the difference between peak luminescence energy in  $\sigma_+$  and  $\sigma_-$  detection, versus magnetic field. For each data point the peak positions were extracted via fits to a phenomenological asymmetric Voigt line shape; other peak shapes were tried with the same results (see supplement section 2). The error bars come primarily from the CCD pixel size (about 0.15 nm per pixel). For both species the valley splitting shows a linear field dependence with a slope of  $-0.22 \pm 0.01 \frac{\text{meV}}{\text{T}}$ , and consistent results were found on three separate devices. The standard deviation between devices was  $0.01 \frac{\text{meV}}{\text{T}}$  for measurements of the exciton splitting and  $0.003 \frac{\text{meV}}{\text{T}}$  for the trion splitting; data from other devices are given in supplement section 3.

Valley splitting in magnetic field arises from the intrinsic chirality of Bloch electrons at the  $K_+$  and  $K_-$  points. States at the two valley edges are Kramer's doublets related by time reversal symmetry, so that their degeneracy can be broken by breaking time reversal sym-

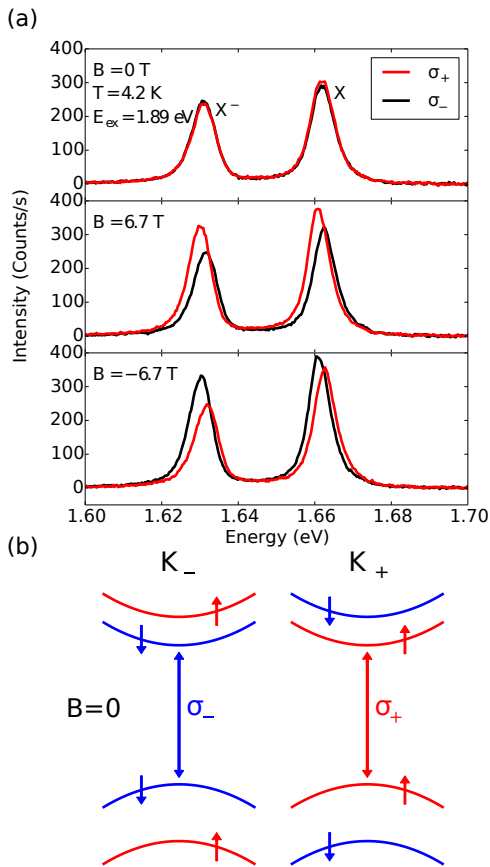


FIG. 2. (a) Polarization-resolved luminescence spectra from monolayer MoSe<sub>2</sub> (D1) at 4.2 K for  $\sigma_+$  (red) and  $\sigma_-$  (black) detection, as excited using unpolarized light at 1.89 eV. From top to bottom the panels show spectra taken with 0 T, 6.7 T and -6.7 T out-of-plane magnetic field. At 6.7 T, the luminescence is  $\sigma_+$  polarized and the  $\sigma_+$  and  $\sigma_-$  peak energies are split by about -1.5 meV. These observations indicate magnetic-field-induced valley degeneracy breaking. Both the polarization and splitting change sign upon reversing the field as shown in the lower panel. (b) Schematic band structure of MoSe<sub>2</sub> near the  $K_+$  and  $K_-$  points in zero magnetic field, showing the optical selection rules for the A exciton transition studied in this experiment. Within each valley, spin degeneracy is broken at  $B = 0$  due to spin-orbit coupling; the valence band splitting is about 180 meV [9, 10], while the conduction band splitting is estimated to be about 20 meV [13, 17, 18].

metry. Physically, Bloch electrons in a given band carry spin and orbital magnetic moments which change sign between valleys [11–13, 19, 20]; Fig. 3b schematically shows the energy shifts arising from Zeeman coupling between these moments and the magnetic field. Magneto-luminescence spectroscopy probes only the exciton Zeeman energy, which is the difference between conduction and valence band Zeeman energies. In this difference, the contributions from bare spin magnetic moments are expected to cancel, leaving only the contributions from

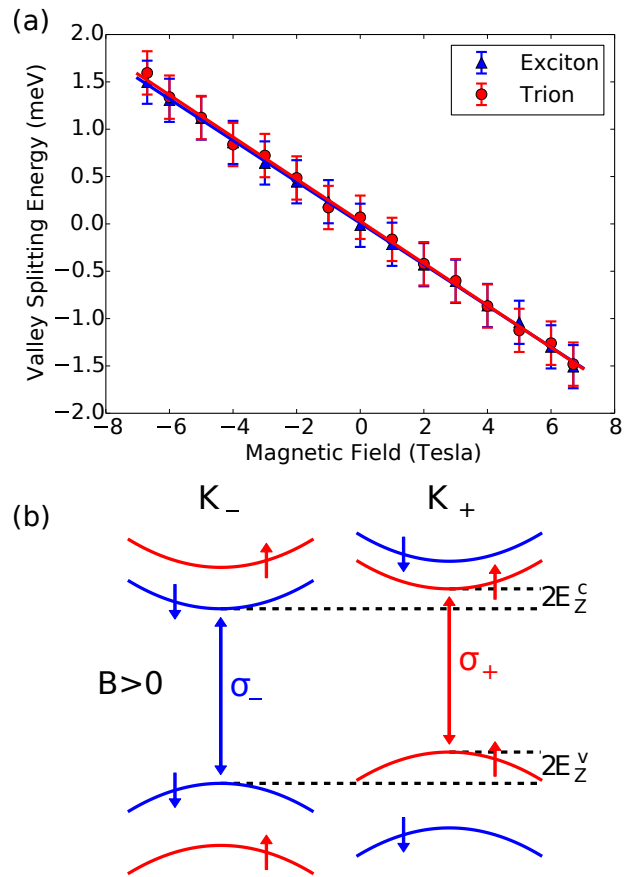


FIG. 3. (a) Difference of peak energies found for  $\sigma_+$  and  $\sigma_-$  detection plotted versus magnetic field for D1. Both the exciton (blue triangles) and trion (red circles) show splitting of  $-0.22 \pm 0.01 \frac{\text{meV}}{\text{T}}$  found via a linear fit. The fits are plotted as blue and red solid lines for the exciton and trion respectively. The linear splitting can be interpreted as twice the Zeeman energy arising from valley-dependent orbital magnetic moments. (b) The schematic band structure of MoSe<sub>2</sub> in magnetic field showing the Zeeman energy  $E_Z^{c(v)}$  for the conduction (valence) band. Our experiment only determines the exciton Zeeman splitting  $2(E_Z^c - E_Z^v)$ , so for this figure we have chosen  $E_Z^c$  and  $E_Z^v$  to be consistent with the sign of the exciton Zeeman splitting.

orbital magnetic moments. For an exciton with valley quantum number  $\tau = \pm 1$  the total Zeeman energy can be decomposed:

$$\frac{1}{2}g_{\text{ex}}^{\text{vl}}\mu_B B\tau = \frac{1}{2}(g_c^{\text{vl}} - g_v^{\text{vl}})\mu_B B\tau \quad (1)$$

where  $g_{c(v)}^{\text{vl}}$  is the valley g-factor for the conduction (valence) band, and  $\mu_B$  is the Bohr magneton. Our measurements give  $g_{\text{ex}}^{\text{vl}} = -3.8 \pm 0.2$ . Considering the trion as an exciton bound to an additional electron, we expect it to have approximately the same splitting as the exciton, consistent with the experimental results of Fig. 3a. While the additional electron contributes to the trion magnetic

moment, it contributes equally to the final state moment after recombination leaving the transition energy unaffected.

According to Eq. 1, a non-zero value for the valley moment only occurs in the presence of electron-hole asymmetry. Specifically, the orbital magnetic moments of the conduction and valence band must differ, which is not the case for the two-band massive Dirac fermion model [12, 21]. Our results can thus test proposals of low-energy Hamiltonians for monolayer TMDs. One can consider calculating the exciton splitting within either a tight-binding approach [20, 22, 23] or a multiband  $\mathbf{k} \cdot \mathbf{p}$  formulation [13, 24]. Our multiband  $\mathbf{k} \cdot \mathbf{p}$  calculation, which makes use of MoSe<sub>2</sub> material parameters obtained from first-principles computations, predicts a splitting magnitude consistent with the measurement, but it appears to predict the opposite sign (see supplement section 4 for our experimental determination of the sign). This work will be published separately.

In addition to the linear shifts as a function of magnetic field discussed above, a magnetic field can also produce a quadratic shift in the exciton binding energy (often called the diamagnetic shift) [25–28], but we calculate that this effect should be negligible in our devices. Our measurements are in the regime where the cyclotron energy (about 1.3 meV at 6.7 T, estimated from DFT effective masses [29]) is much smaller than the exciton binding energy (550 meV [30]), so that the magnetic field can be considered a perturbation to the exciton Hamiltonian. In supplement section 5 we estimate the resulting quadratic shift using the Wannier model and find that it is on the order of 10  $\mu\text{V}$  and therefore below our measurement sensitivity.

To investigate the gate dependence of valley splitting and polarization, we turn to data from device D2. Polarization-resolved spectra taken with -20 V and 51 V applied to the substrate are shown in Fig. 4a. Our devices show significant hysteresis assumed to arise from photoionization of trap states [31], and the data in this panel are taken from a downward sweep. Figure 4b shows the trion splitting versus magnetic field for two different gate voltages on a downward sweep, finding  $-0.29 \frac{\text{meV}}{\text{T}}$  at 40 V and  $-0.23 \frac{\text{meV}}{\text{T}}$  at 0 V. Changes in the trion splitting with charge density might arise from  $\mathbf{k}$  dependence of the g-factor or valley-dependent exchange coupling due to valley polarization of the electron gas.

Another unexpected feature is an increase in the degree of trion polarization as a function of gate voltage, as shown in Fig. 4c. We find a trion polarization of over 50% at our highest back gate voltages. The trion polarization in the  $n$ -type regime further increases to about 65% as the excitation power is reduced (see supplement section 6). Naively, the luminescence polarization is related to the valley population via  $\frac{I_+ - I_-}{I_+ + I_-} = \frac{n_+ - n_-}{n_+ + n_-}$ , where  $n_{\pm}$  is the trion population in valley  $K_{\pm}$ . From this we infer

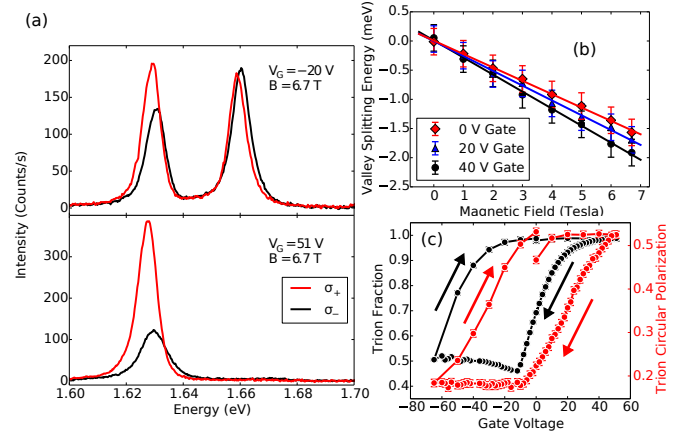


FIG. 4. (a) Polarization-resolved luminescence spectra from D2 at 4.2K and 6.7 T for  $\sigma_+$  (red) and  $\sigma_-$  (black) detection, excited with  $\sigma_-$  light at 1.89 eV. From top to bottom the panels show spectra taken with -20 V and 51 V gate voltage applied to the substrate. (b) Valley splitting versus field for selected gate voltages, showing an decrease in slope with gate voltage. (c) Circular polarization of the trion peak  $\frac{I_+ - I_-}{I_+ + I_-}$  versus gate voltage (red), showing an increase to over 50% as gate voltage is increased. For comparison, we plot the trion fraction  $\frac{I_{\text{trion}}}{I_{\text{trion}} + I_{\text{exciton}}}$  in black.

that we are observing the generation of valley-polarized trion populations through applied magnetic field and gate voltage. We have not determined the origin of this effect, but expect the gate dependence of the trion formation and intervalley scattering times along with the free carrier valley polarization to play a role [32]. The data in Fig. 4 were taken with  $\sigma_-$  polarized excitation, but we obtained similar results for another device using unpolarized excitation (see supplement section 3).

In summary, we have presented measurements of polarization-resolved luminescence spectra for MoSe<sub>2</sub> at 4.2 K in magnetic fields up to 6.7 T, demonstrating valley degeneracy breaking. We measure a splitting of  $-0.22 \pm 0.01 \frac{\text{meV}}{\text{T}}$  between peaks in  $\sigma_+$  and  $\sigma_-$  polarized emission spectra. Our results cannot be accounted for within an electron-hole symmetric theory, and thus probe the TMD band structure beyond the simple two-band massive Dirac fermion model [12, 21]. Measurements of the exciton valley splitting therefore provide a testing ground for understanding electron-hole asymmetry in monolayer TMDs. Further tests may come from absorption spectroscopy, which allows measurement of the B exciton valley moment. This is expected to differ from the A exciton studied here due to spin-orbit coupling [13], which leads to spin dependence of the orbital magnetic moments, similar to the origin of effective spin g-factors in other spin-orbit coupled semiconductors. Comparison of the A and B exciton splittings should then improve our understanding of the origin of valley degen-

eracy breaking.

We also observe gate dependence of the valley splitting and luminescence handedness. Even with off-resonant, unpolarized excitation we were able to achieve trion circular polarization of about 50% by gating the sample in 6.7 T magnetic field, demonstrating the generation of valley-polarized populations through valley degeneracy breaking. Future measurements on devices with both top and back gates might help to determine whether this effect arises from the external electric field or the changing Fermi level. Out-of-plane electric fields break horizontal mirror symmetry, and have been predicted to modify the valley splitting and change the nature of spin-orbit coupling, which could give rise to magnetoelectric effects in sufficiently strong electric fields and provide additional strategies for control over the valley degree of freedom [13, 20].

We thank Kathryn McGill and Joshua Kevek for growth of the bulk MoSe<sub>2</sub> crystal used for this work. We also thank Guido Burkard, Péter Rakyta, Alexander Högele and Ermin Malic for helpful discussions. This research was supported in part by the NSF (DMR-1010768) and the Kavli Institute at Cornell for Nanoscale Science. We also made use of the Cornell Center for Materials Research Shared Facilities which are supported through the NSF MRSEC program (DMR-1120296). Device fabrication was performed at the Cornell NanoScale Facility, a member of the National Nanotechnology Infrastructure Network, which is supported by the National Science Foundation (Grant ECCS-0335765). D. M. acknowledges support from a NSERC PGS scholarship.

- 
- [1] D. Xiao, G.-B. Liu, W. Feng, X. Xu, and W. Yao, *Phys. Rev. Lett.* **108**, 196802 (2012).
- [2] K. F. Mak, K. He, J. Shan, and T. F. Heinz, *Nat. Nanotech.* **7**, 494 (2012).
- [3] A. M. Jones, H. Yu, N. J. Ghimire, S. Wu, G. Aivazian, J. S. Ross, B. Zhao, J. Yan, D. G. Mandrus, D. Xiao, *et al.*, *Nat. Nanotech.* **8**, 634 (2013).
- [4] G. Kioseoglou, A. Hanbicki, M. Currie, A. Friedman, D. Gunlycke, and B. Jonker, *App. Phys. Lett.* **101**, 221907 (2012).
- [5] H. Zeng, J. Dai, W. Yao, D. Xiao, and X. Cui, *Nat. Nanotech.* **7**, 490 (2012).
- [6] T. Cao, G. Wang, W. Han, H. Ye, C. Zhu, J. Shi, Q. Niu, P. Tan, E. Wang, B. Liu, *et al.*, *Nat. Commun.* **3**, 887 (2012).
- [7] G. Sallen, L. Bouet, X. Marie, G. Wang, C. R. Zhu, W. P. Han, Y. Lu, P. H. Tan, T. Amand, B. L. Liu, and B. Urbaszek, *Phys. Rev. B* **86**, 081301 (2012).
- [8] K. F. Mak, K. L. McGill, J. Park, and P. L. McEuen, *ArXiv e-prints* (2014), arXiv:1403.5039 [cond-mat.mes-hall].
- [9] J. S. Ross, S. Wu, H. Yu, N. J. Ghimire, A. M. Jones, G. Aivazian, J. Yan, D. G. Mandrus, D. Xiao, W. Yao, *et al.*, *Nat. Commun.* **4**, 1474 (2013).
- [10] Y. Zhang, T.-R. Chang, B. Zhou, Y.-T. Cui, H. Yan, Z. Liu, F. Schmitt, J. Lee, R. Moore, Y. Chen, *et al.*, *Nat. Nanotech.* **9**, 111 (2013).
- [11] D. Xiao, W. Yao, and Q. Niu, *Phys. Rev. Lett.* **99**, 236809 (2007).
- [12] W. Yao, D. Xiao, and Q. Niu, *Phys. Rev. B* **77**, 235406 (2008).
- [13] A. Kormányos, V. Zólyomi, N. D. Drummond, and G. Burkard, *Phys. Rev. X* **4**, 011034 (2014).
- [14] T. Cai, S. A. Yang, X. Li, F. Zhang, J. Shi, W. Yao, and Q. Niu, *Phys. Rev. B* **88**, 115140 (2013).
- [15] A. Högele, S. Seidl, M. Kroner, K. Karrai, C. Schülhauser, O. Sqalli, J. Scrimgeour, and R. J. Warburton, *Rev. Sci. Instrum.* **79**, 023709 (2008).
- [16] M. Sladkov, M. Bakker, A. Chaubal, D. Reuter, A. Wieck, and C. van der Wal, *Review of Scientific Instruments* **82**, 043105 (2011).
- [17] G.-B. Liu, W.-Y. Shan, Y. Yao, W. Yao, and D. Xiao, *Phys. Rev. B* **88**, 085433 (2013).
- [18] K. Kośmider, J. W. González, and J. Fernández-Rossier, *Phys. Rev. B* **88**, 245436 (2013).
- [19] M.-C. Chang and Q. Niu, *J. Phys.: Condens. Matter* **20**, 193202 (2008).
- [20] H. Rostami, A. G. Moghaddam, and R. Asgari, *Phys. Rev. B* **88**, 085440 (2013).
- [21] X. Li, F. Zhang, and Q. Niu, *Phys. Rev. Lett.* **110**, 066803 (2013).
- [22] R.-L. Chu, X. Li, S. Wu, Q. Niu, X. Xu, and C. Zhang, *arXiv preprint arXiv:1401.4806* (2014).
- [23] Y.-H. Ho, Y.-H. Wang, and H.-Y. Chen, *Phys. Rev. B* **89**, 155316 (2014).
- [24] A. Kormányos, V. Zólyomi, N. D. Drummond, P. Rakyta, G. Burkard, and V. I. Fal'ko, *Phys. Rev. B* **88**, 045416 (2013).
- [25] N. Gippius, A. Yablonskii, A. Dzyubenko, S. Tikhodeev, L. Kulik, V. Kulakovskii, and A. Forchel, *J. Appl. Phys.* **83**, 5410 (1998).
- [26] M. Sugawara, N. Okazaki, T. Fujii, and S. Yamazaki, *Phys. Rev. B* **48**, 8848 (1993).
- [27] H. Q. Hou, W. Staguhn, S. Takeyama, N. Miura, Y. Segawa, Y. Aoyagi, and S. Namba, *Phys. Rev. B* **43**, 4152 (1991).
- [28] D. C. Rogers, J. Singleton, R. J. Nicholas, C. T. Foxon, and K. Woodbridge, *Phys. Rev. B* **34**, 4002 (1986).
- [29] A. Ramasubramaniam, *Phys. Rev. B* **86**, 115409 (2012).
- [30] M. M. Ugeda, A. J. Bradley, S.-F. Shi, F. H. da Jornada, Y. Zhang, D. Y. Qiu, S.-K. Mo, Z. Hussain, Z.-X. Shen, F. Wang, *et al.*, *arXiv preprint arXiv:1404.2331* (2014).
- [31] A. A. Mitioğlu, P. Plochocka, J. N. Jadczyk, W. Escoffier, G. L. J. A. Rikken, L. Kulyuk, and D. K. Maude, *Phys. Rev. B* **88**, 245403 (2013).
- [32] C. R. L. P. N. Jeukens, P. C. M. Christianen, J. C. Maan, D. R. Yakovlev, W. Ossau, V. P. Kochereshko, T. Wojtowicz, G. Karczewski, and J. Kossut, *Phys. Rev. B* **66**, 235318 (2002).
- [33] J. Ma and Y.-S. Li, *Applied optics* **35**, 2527 (1996).
- [34] A. Mal'yavkin, *Solid State Communications* **39**, 1315 (1981).
- [35] E. Molva and L. S. Dang, *Physical Review B* **27**, 6222 (1983).
- [36] E. Molva and L. S. Dang, *Physical Review B* **32**, 1156 (1985).
- [37] R. S. Knox, *Theory of excitons*, Vol. 5 (Academic Press New York, 1963).



- [38] G. Berghäuser and E. Malic, Phys. Rev. B **89**, 125309 (2014).  
 [39] A. Chernikov, T. C. Berkelbach, H. M. Hill, A. Rigosi, Y. Li, O. B. Aslan, D. R. Reichman, M. S. Hybertsen,

- and T. F. Heinz, arXiv preprint arXiv:1403.4270 (2014).  
 [40] C. Zhang, H. Wang, W. Chan, C. Manolatou, and F. Rana, Phys. Rev. B **89**, 205436 (2014).  
 [41] T. C. Berkelbach, M. S. Hybertsen, and D. R. Reichman, Phys. Rev. B **88**, 045318 (2013).

## Supplement to “Valley degeneracy breaking by magnetic field in monolayer MoSe<sub>2</sub>”

### 1. Dependence of Luminescence Handedness on Excitation Handedness

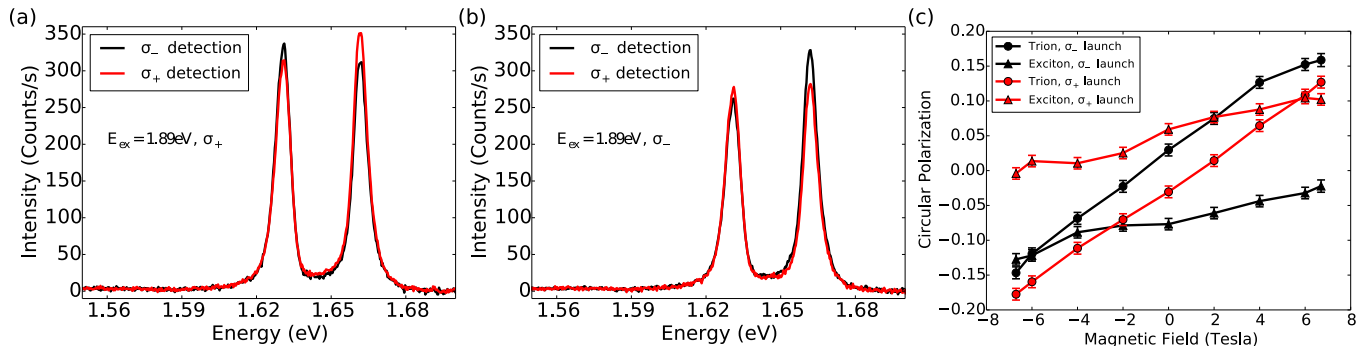


FIG. 5. (a) Polarization-resolved spectra from D1 taken at zero magnetic field and with  $\sigma_+$  excitation, showing  $\sigma_+$  polarization of exciton luminescence. (b) Polarization-resolved spectra from D1 taken at zero magnetic field and with  $\sigma_-$  excitation. (c) Luminescence polarization versus magnetic field with  $\sigma_+$  (red) and  $\sigma_-$  (black) excitation for excitons (triangles) and trions (circles).

Figures 5a and 5b show polarization-resolved luminescence spectra for D1 at  $T = 4.2$  K and  $B = 0$  T taken with  $\sigma_+$  and  $\sigma_-$  polarized excitation respectively. We observe some preservation of the incident polarization even with our 1.89 eV excitation. We find  $P_{\text{exciton}} = \frac{I_+ - I_-}{I_+ + I_-} = 6\%$  for  $\sigma_+$  excitation and  $P_{\text{exciton}} = -8\%$  for  $\sigma_-$  excitation indicating 7% average co-polarization of exciton luminescence with the excitation laser. On the other hand, we see counter polarization of 3% for the trion luminescence. We also studied the dependence of the field-induced polarization on excitation handedness: as shown in Fig. 5c switching the excitation polarization seemingly adds a constant offset. The small polarization preservation we observe is consistent with studies of polarization preservation in MoS<sub>2</sub> using off-resonant excitation [2, 4].

### 2. Background Subtraction and Fitting

Raman scattering of the excitation laser in the fiber presents a significant background in our experiment, as has been reported elsewhere [15, 33]. A spectrum of fiber Raman excited with 705 nm light is plotted in Fig. 6a, showing fused silica Raman peaks [33]. Since we excite with 656 nm light we encounter only the tail of this signal during measurements of MoSe<sub>2</sub> luminescence. To account for this background, we take additional spectra with the excitation laser spot on silicon; the background spectrum is then subtracted from the signal after carrying out a dark count subtraction on both spectra. This is shown in Figs. 6b and 6c. In practice, we rescale the background to match the signal spectrum away from the luminescence peaks, to account for laser power fluctuations and to allow a single background spectrum to be used multiple times. In Figs. 6b and 6c we have used the data without rescaling to prove that fiber Raman entirely accounts for the background.

In the main text we report values for the peak polarization and energy as a function of magnetic field and gating. As described there, we use fits to an asymmetric Voigt profile to extract the peak properties. The Voigt function is defined as

$$\frac{1}{\sigma\sqrt{2\pi}} \operatorname{Re} \left\{ \exp \left[ - \left( \frac{\delta\omega + i\gamma}{\sqrt{2}\sigma} \right)^2 \right] \operatorname{erfc} \left[ -i \left( \frac{\delta\omega + i\gamma}{\sqrt{2}\sigma} \right) \right] \right\}, \quad (2)$$

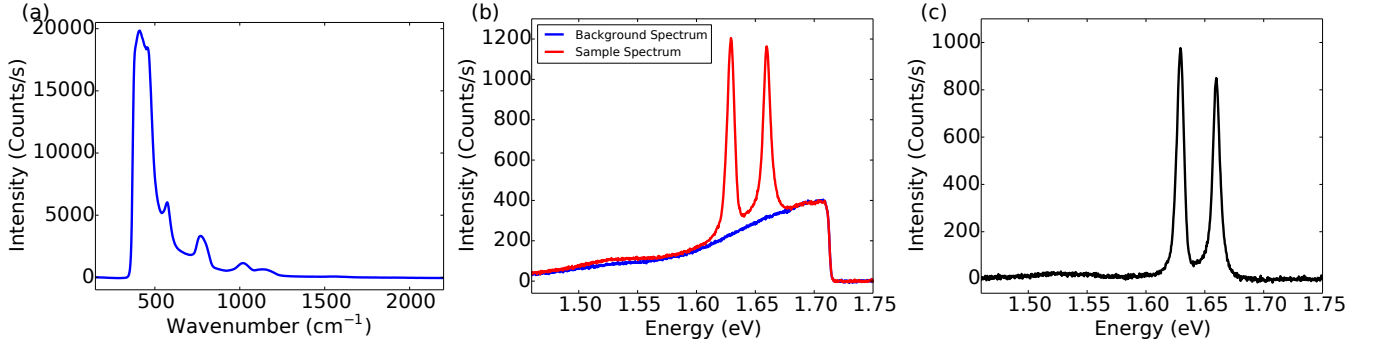


FIG. 6. (a) Fiber background spectrum excited with 705 nm laser diode, showing fused silica Raman peaks. (b) Comparison of spectra taken with 656 nm excitation laser on the sample (red) and on a nearby region of bare substrate (blue). (c) The result of subtracting the two curves in (b).

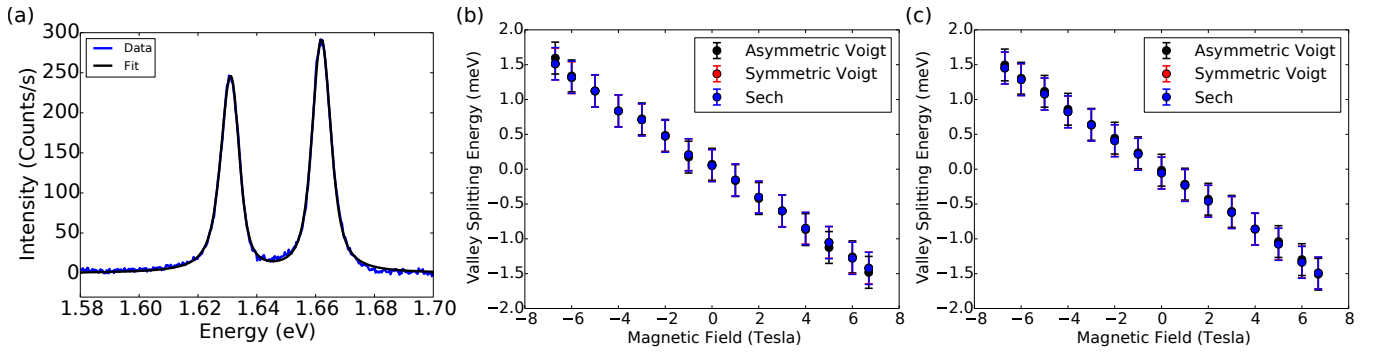


FIG. 7. (a) Comparison of sample luminescence spectrum (blue) and fit used to locate peak energy (black). The spectrum is fit to the sum of two asymmetric Voigt profiles, with  $\chi^2 \approx 3$  (b) Trion valley splitting as extracted with fits to asymmetric Voigt (black), symmetric Voigt (red), and hyperbolic secant (blue). (c) Exciton valley splitting as extracted with fits to asymmetric Voigt (black), symmetric Voigt (red), and hyperbolic secant (blue). Valley splittings from asymmetric Voigt fits are presented in Fig. 3 of the main text.

where  $\delta\omega$  is the detuning and  $\gamma$  and  $\sigma$  are fit parameters characterizing the peak width. As written, the function describes the convolution of a Lorentzian with width  $\gamma$  and a Gaussian with width  $\sigma$ ; to make the line shape asymmetric we allow  $\gamma$  to take different values for positive and negative detuning. A typical spectrum with fit is plotted in Fig. 7a; in this case the  $\chi^2$  was about 3. We also tried fitting to other functions, such as a hyperbolic secant and a symmetric Voigt profile. There was no difference in the valley splitting within our errorbars. A comparison of splitting energies between symmetric Voigt, hyperbolic secant and asymmetric Voigt is shown in Figs. 7b and 7c.

### 3. Comparison of Data from Multiple Devices

We measured the valley splitting versus magnetic field with the back gate grounded for three different devices. All data were taken at 4.2 K and with 1.89 eV excitation. Valley splitting data not shown in the main text are given in Fig. 8; D1 and D2 are defined in the main text, and the additional device is called D3. For D3, we took data at two different positions on the flake. We have also provided Table I showing the slopes extracted from linear fits to this data. The standard deviation across samples of the trion splitting is  $0.003 \frac{\text{meV}}{\text{T}}$  and the standard deviation of the exciton splitting is  $0.01 \frac{\text{meV}}{\text{T}}$ . These values are within the systematic error estimated from the CCD pixel size. For one of the locations on D3, there was a significant discrepancy between the exciton and trion splitting.

We also measured the gate dependence of valley splitting and polarization on two devices: D2 and another device not previously defined, D4. The gate dependence of luminescence from D4 is shown in Fig. 9. As shown in Fig. 9a, for D4 the trion polarization increases from about 10% to over 45% as the electron density is increased. For the data

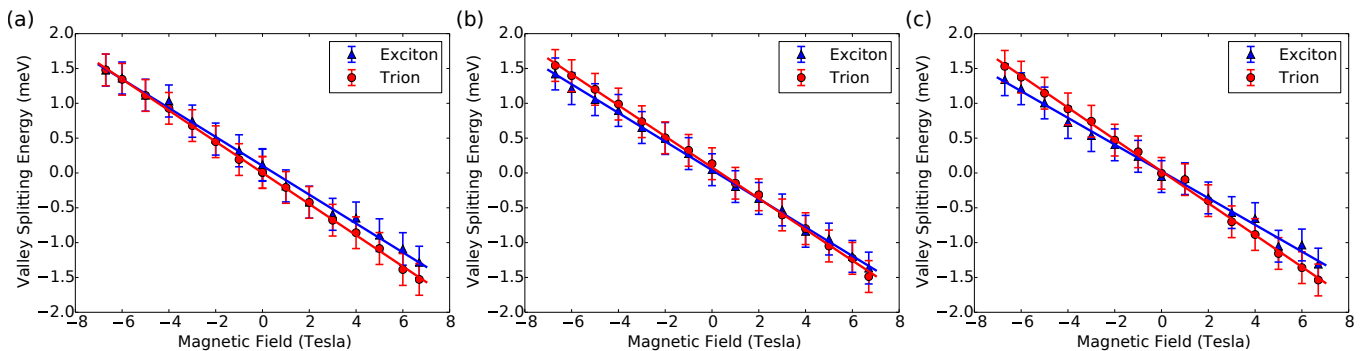


FIG. 8. (a) Valley splitting data for D1, as defined in the main text. (b) Valley splitting data taken near the center of D3. (c) Valley splitting data taken near one edge of D3.

Sample	Exciton Splitting ( $\frac{\text{meV}}{\text{T}}$ )	Trion Splitting ( $\frac{\text{meV}}{\text{T}}$ )
D1	-0.22	-0.22
D2	-0.21	-0.22
D3 location 1	-0.21	-0.22
D3 location 2	-0.19	-0.23

TABLE I. Valley splitting for multiple devices in  $\frac{\text{meV}}{\text{T}}$ , defined as the difference of luminescence peak energies between  $\sigma_+$  and  $\sigma_-$  polarized light. The error for all values is  $\pm 0.01 \frac{\text{meV}}{\text{T}}$ .

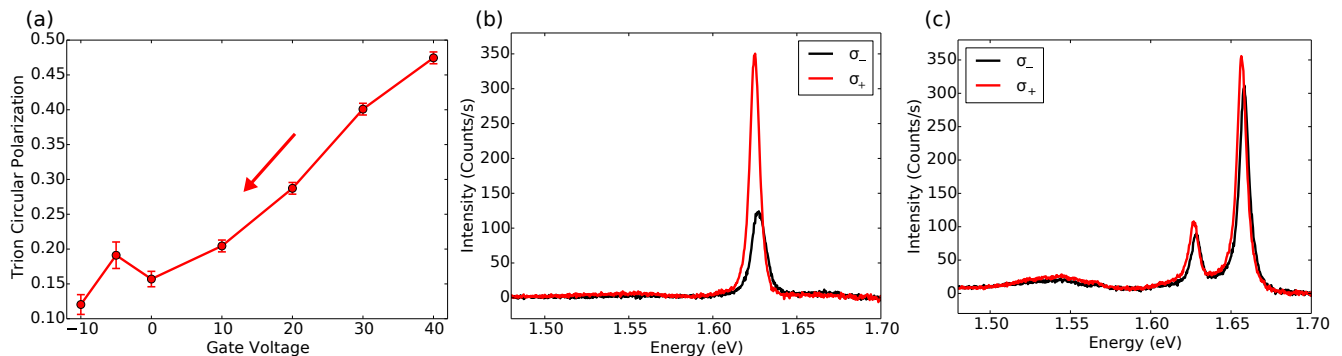


FIG. 9. (a) Trion peak polarization versus gate voltage at  $B = 6.7$  T for D4 taken on a downward sweep and using  $11 \mu\text{W}$  excitation with equal intensity in  $\sigma_+$  and  $\sigma_-$  light (b) Polarization-resolved luminescence spectrum of D4 taken at 6.7 T magnetic field and 40 V back gate voltage. (c) Polarization-resolved luminescence spectrum of D4 taken at 6.7 T magnetic field and -20 V back gate voltage. The trion polarization is significantly reduced compared to the 40 V spectrum.

in Fig. 9 we used excitation light with equal intensity in  $\sigma_+$  and  $\sigma_-$  polarization, and about  $11 \mu\text{W}$  excitation power.

#### 4. Determination of the Sign of the Valley Splitting

In the main text, we define the valley splitting as the difference of peak luminescence energies between  $\sigma_+$  and  $\sigma_-$  polarized emission. Furthermore,  $\sigma_{\pm}$  polarization is defined as the circular polarization which carries  $\pm\hbar$  angular momentum per photon along the field direction for  $B > 0$ . Equivalently,  $\sigma_+$  ( $\sigma_-$ ) polarized light can be defined as the light with electric field vector rotating counter-clockwise (clockwise) in time around the positive  $B$  axis. The convention for  $B > 0$  is defined in Fig. 1a of the main text. To determine the sign of the splitting, we used two methods.

First, we determined the rotational settings of the detection polarizer corresponding to different circular polariza-



tions of emission. To do this, we launched circularly-polarized laser light into the cryostat objective lens from the sample space, and found the settings of the detection polarizer which maximized the resulting signal. The circularly polarized light was generated by sending linearly polarized light through a  $\lambda/4$  plate with the light polarized at  $45^\circ$  to the waveplate axes. Given knowledge of the waveplate axes and their orientation relative to the light polarization, the handedness of circularly polarized light produced in this fashion can be determined. We also checked the assignment of the waveplate fast and slow axes by shining circularly polarized light of a known handedness through the waveplate and analyzing the resulting linear polarization. For this test, the circularly polarized light was generated using two N-BK7 prisms in a Fresnel rhomb geometry, so that the resulting handedness could be determined from the Fresnel equations. We determined the field direction using a calibrated Hall probe. The considerations above determine the rotational settings of the detection polarizer corresponding to detection of  $\sigma_+$  and  $\sigma_-$  emission.

We also compared the valley splitting for MoSe<sub>2</sub> to magnetoluminescence measurements for a (110) cut, undoped, *p*-type CdTe substrate (from MTI Corporation). For *p*-type CdTe, the acceptor-bound exciton luminescence shows a four-fold splitting under magnetic field applied in the Faraday geometry. The optical selection rules lead to circular polarization of these peaks, so that two are  $\sigma_+$  polarized and two are  $\sigma_-$  polarized. With the detection polarization determined as discussed above, we find peak splitting and selection rules for CdTe in agreement with those found by Refs. [34–36]. In particular, given that the lowest energy acceptor-bound exciton luminescence peak for CdTe is  $\sigma_-$  polarized (for  $B > 0$ ), we know that the lowest energy MoSe<sub>2</sub> peak indeed originates from  $\sigma_+$  polarized luminescence (for  $B > 0$ ) as indicated in the main text.

### 5. Exciton Hamiltonian for MoSe<sub>2</sub> in magnetic fields

The exciton Hamiltonian is found by subtracting the conduction and valence band dispersions (see Ref. [13] for a derivation of the effective conduction band Hamiltonian in magnetic field) and adding the electron-hole Coulomb interaction  $V$ :

$$H_{\text{ex}} = H_c(\mathbf{q}_c) - H_v(\mathbf{q}_v) + V(|\mathbf{r}_c - \mathbf{r}_v|) = \frac{\hbar^2}{2m_c}\mathbf{q}_c^2 - \frac{\hbar^2}{2m_v}\mathbf{q}_v^2 + V(|\mathbf{r}_c - \mathbf{r}_v|) + \frac{1}{2}g_{\text{ex}}^{\text{vl}}\mu_B B\tau. \quad (3)$$

where  $m_{c(v)}$  is the effective mass for the conduction (valence) band,  $\tau = \pm 1$  indicates the exciton valley quantum number, and  $g_{\text{ex}}^{\text{vl}} = g_c^{\text{vl}} - g_v^{\text{vl}}$  is the valley *g*-factor discussed in the main text. In magnetic fields,  $\mathbf{q}_b = \mathbf{p}_b + e\mathbf{A}(\mathbf{r}_b)$  where  $\mathbf{p}_b$  is the canonical momentum and  $\mathbf{A}(\mathbf{r}) = \frac{B}{2}\hat{z} \times \mathbf{r}$ . Following Refs. [25, 37], we carry out a gauge transformation to find a one-body Hamiltonian for excitons with zero center of mass momentum:

$$H_{\text{ex}}^\tau = \frac{\hbar^2}{2\mu}\mathbf{p}^2 + \frac{\hbar e B}{2}\left(\frac{1}{m_c} - \frac{1}{|m_v|}\right)l_z + \frac{e^2 B^2}{8\mu}\mathbf{r}^2 + V(|\mathbf{r}|) + \frac{1}{2}g_{\text{ex}}^{\text{vl}}\mu_B B\tau \quad (4)$$

where  $\mathbf{r} = \mathbf{r}_c - \mathbf{r}_v$  is the electron-hole separation,  $\mathbf{p}$  is the associated canonical momentum,  $\mu = m_c|m_v|/(m_c + |m_v|)$ , and  $l_z = \hat{z} \cdot (\mathbf{r} \times \mathbf{p})$ . For bright excitons we assume  $l_z = 0$ , i.e. that they are *s*-type [38–41]. Therefore the only term which can give rise to a linear magnetic field dependence of the exciton energy is the last term in Eq. 4, which describes a Zeeman-like coupling of the valley degree of freedom to the magnetic field.

In the regime where the magnetic length ( $l_B = \sqrt{\frac{\hbar}{eB}}$ ) is smaller than the exciton Bohr radius, magnetic confinement leads to a quadratic shift of the exciton transition energy as demonstrated in experiments on quantum wells [25–28]. Theoretically, this could manifest in our experiments as a quadratic term in the valley averaged transition energy, but due to the small exciton Bohr radius for TMDs (1–3 nm [39–41]) the correction should be small. We can estimate the diamagnetic shift using perturbation theory and the Wannier model above: the result is a quadratic increase of order  $\frac{1}{8}\hbar(\omega_c + \omega_v)\left(\frac{a_B}{l_B}\right)^2 \approx 7 \mu\text{eV}$  at 6.7 T, where  $\omega_{c(v)}$  is the electron (hole) cyclotron frequency, and  $a_B$  is the exciton Bohr radius. This estimate is consistent with absence of any trend in our data for the valley averaged transition energy.

### 6. Power Dependence of Trion polarization

As shown in Fig. 10a, the trion luminescence polarization increases to about 65% circularly polarized as the power is reduced for  $B = 6.7$  T,  $T = 4.2$  K, and in the regime of high electron density. On the other hand, we see no power dependence of the trion peak splitting (see Fig. 10b). The power dependence of trion polarization may result from changes in the lattice temperature, or the effective temperature of the trion population which is likely not in

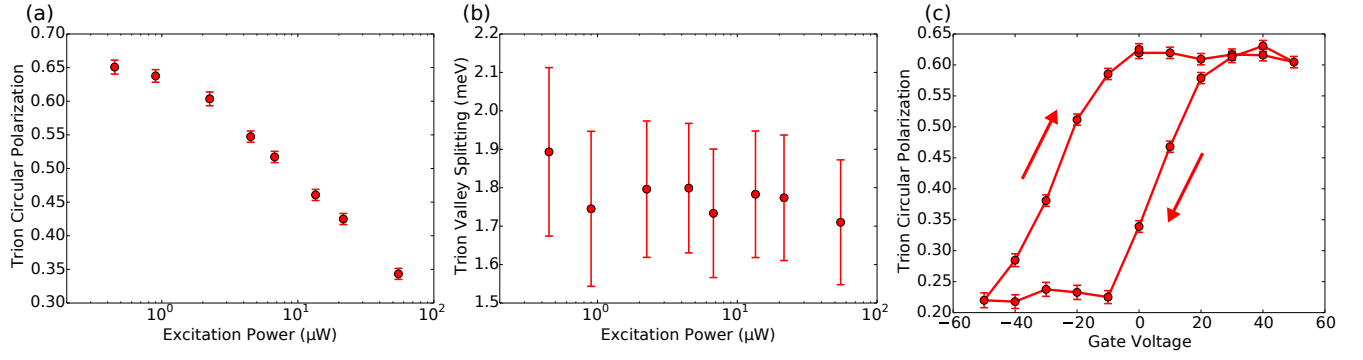


FIG. 10. (a) Trion peak circular polarization versus power in the  $n$ -type regime, for  $B = 6.7$  T, and excited with  $\sigma_-$  polarized light. (b) Trion valley splitting versus power in the  $n$ -type regime and for  $B = 6.7$  T. (c) Trion peak circular polarization versus gate voltage, taken at 6.7 T and using about  $1.1 \mu\text{W}$  excitation power.

equilibrium with the lattice. A thermometer mounted on the chip holder shows  $< 50$  mK sample heating under more than  $200 \mu\text{W}$  excitation, suggesting that the lattice heating is small. Figure 10c shows the gate dependence of trion polarization at 6.7 T and 4.2 K, with an excitation power of about  $1.1 \mu\text{W}$ ; the fractional increase in the trion polarization with gate voltage is similar to data shown in the main text (taken with about  $11 \mu\text{W}$  excitation).